Journal of Biomolecular NMR, **167:** 167–172, 2001.
KLUWER/ESCOM

Novel 2D and 3D multiple-quantum bi-directional HCNCH experiments for the correlation of ribose and base protons/carbons in $^{13}C/^{15}N$ labeled RNA

Weidong Hu*, Yuying Q. Gosser, Weijun Xu & Dinshaw J. Patel
Memorial Sloan-Kettering Cancer Center, 1275 York Avenue, New York, NY 10021, U.S.A.

Received 8 February 2001; Accepted 20 March 2001

Key words: base-sugar proton/carbon correlation, bi-directional HCNCH, multiple-quantum coherence, RNA oligomers

Abstract

Multiple-quantum 2D and 3D bi-directional HCNCH experiments are presented for the correlation of base and ribose protons/carbons in $^{13}C/^{15}N$ labeled HIV-1 TAR RNA. In both 2D and 3D experiments, the magnetization of H1′ is transferred to H6/H8 and H1′ through H1′-C1′-N1/9-C6/8-H6/8 and H1′-C1′-N1/9-C1′-H1′ pathways, and the magnetization of H6/8 is transferred to H1′ and H6/8 through H6/8-C6/8-N1/9-C1′-H1′ and H6/8-C6/8-N1/9-C6/8-H6/8 pathways. Chemical shifts of four different nuclei (H1′, C1′, C6/8 and H6/8) are sampled in the 2D experiment. The correlation of base and ribose protons/carbons is established by the rectangular arrangement of crossover and out-and-back peaks in the proton/carbon correlated spectrum. The rectangular connections can be further resolved using the nitrogen dimension in a $^{1}H/^{13}C/^{15}N$ 3D experiment. Furthermore, by taking advantage of the well separated chemical shifts of N1 (pyrimidine) and N9 (purine), the 2D spectrum can be simplified into two sub-spectra based on their base type. Both experiments were tested on a $^{13}C/^{15}N$ labeled 27-mer HIV-1 TAR RNA containing a UUCG hairpin loop.

With the advent of isotopic labeling techniques for the preparation of $^{13}C/^{15}N$-labeled nucleic acids (Batey et al., 1992; Nikonowicz et al., 1992; Michnicka et al., 1993), the correlation of base and ribose positions can be achieved more reliably from hetero-nuclear correlation experiments instead of NOESY experiments (Wüthrich, 1986). Experiments which correlate base and ribose resonances through the H1′-C1′-N1/9-C6/8-H6/8 moiety with different chemical shift labeling schemes and coherence transfer pathways have been published. These studies include 2D and 3D $H_sC_sN_b$ and $H_bC_bN_b$ experiments (Sklenár et al., 1993a; Farmer et al., 1994), where the s and b stand for the nuclei in sugar and base, 3D $H_sC_s(N_bC_b)H_b$ (Farmer et al., 1993), 2D $H_s(C_sN_bC_b)H_b$ (Sklenár et al., 1993b), 2D $H_s(C_sN_b)H_b$ for purine (Tate et al., 1994), 3D $H_sC_s(N_b)C_b$ (Farmer et al., 1994) and 3D $H_s(C_s)N_b(C_b)H_b$ (Fiala et al., 1998). The $H_sC_sN_b$ and $H_bC_bN_b$ experiments together establish the base-ribose correlation through the N_b position. The 3D $H_sC_s(N_bC_b)H_b$, 2D $H_s(C_sN_bC_b)H_b$, 2D $H_s(C_sN_b)H_b$ and $H_s(C_s)N_b(C_b)H_b$ connect the base and ribose through the H_s and H_b correlation. The 3D $H_sC_s(N_b)C_b$ experiment connects the base and ribose through the H_s and C_b correlation. All these experiments only sample chemical shifts of two or three different nuclei. While this communication was in preparation, a new 3D experiment was reported which samples both $H_sC_sN_b$ and $H_bC_bN_b$ simultaneously (Riek et al., 2001). The experiment uses an out-and-back scheme, thus base-ribose correlation relies solely on N_b. The potential obstacle for the base-ribose correlation using the experiments mentioned above comes from the fact that the chemical shifts of C1′ and H1′ are generally severely overlapped, and those of C6/8 and H6/8 are generally not well dispersed. It would be

*To whom correspondence should be addressed. E-mail: weidong@sbnmr1.ski.mskcc.org

advantageous to make use of as many different nuclei as possible in a single experiment to establish multiple connections between base and ribose positions in order to reduce the ambiguity.

Compared to the NOESY-type experiment, sensitivity of the triple-resonance experiments correlating base and ribose through scalar couplings is hampered by the small couplings of C1′-N1/9 and C6/8-N1/9. This drawback has been alleviated to a great extent through the slower relaxation rate associated with multiple-quantum coherence experiments as well as the TROSY techniques (Grzesiek and Bax, 1995; Grzesiek et al., 1995; Marino et al., 1997; Fiala et al. 1998, 2000; Sklenár et al., 1998; Riek et al., 2001). On the other hand, compared to 3D experiments, more signal averaging is feasible in a 2D experiment, provided that overlap is not a problem.

Simultaneous sampling of $^{13}C/^{1}H$ and $^{15}N/^{1}H$ correlations has been reported for protein samples by several groups (Sørensen, 1990; Farmer and Müller, 1991; Boelens et al., 1994; Mariani et al., 1994; Sattler et al., 1995). These methods significantly shorten data collection time and provide more information content when used in 3D and 4D experiments (Farmer and Müller, 1994; Mariani et al., 1994; Pascal et al., 1994). More recently, a bi-directional 3D HNHCACO experiment (Pang et al., 1998) and a sensitivity-enhanced $HNCA^{+}$ scheme using two different coherence pathways (Salzmann et al., 2000) for protein backbone assignment were introduced. While this paper was in preparation, a TROSY version of the 3D HCN experiment which simultaneously monitors both H1′-C1′-N1/9 and H6/8-C6/8-N1/9 pathways in an out-and-back manner was published (Riek et al., 2001).

In this paper we present a novel bi-directional HCNCH experiment (bid-HCNCH), with 2D and 3D versions, to establish the correlation of base and ribose positions. The pulse sequences for 2D and 3D bid-HCNCH experiments are shown in Figures 1A and 1B. The magnetization transfer steps for the 3D bid-HCNCH will be described briefly using the product operator formalism (Sørensen et al., 1983). The magnetization flow chart of the 3D bid-HCNCH experiment (Figure 1B) is as follows:

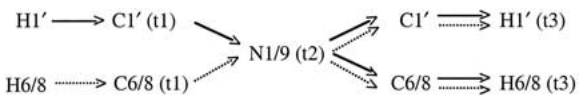

where the solid and the dotted arrows stand for the magnetization that starts from H1′ and H6/8, respectively. As shown in the scheme above, the magnetization starting from H1′ ends up at both H1′ and H6/8, and that from H6/8 also ends up at both H1′ and H6/8. Since the coherence pathways starting from H1′ and H6/8 are symmetrical, the following discussion will focus on the one starting from H1′ only. At point a, the 90° pulse on carbon generates a multiple quantum term of $C1'_yH1'_x$. From point a to c, the chemical shift of C1′ is labeled, the scalar coupling interaction between C1′ and C2′ is refocused by the two I-BURP 180° pulses (Geen and Freeman, 1991) on C2′, and the antiphase term of C1′ to N1/9 is developed. The chemical shift of H1′ is refocused from point a to b, and the multiple quantum term of C1′ to H1′ is converted to antiphase by the 90° pulse on proton at point b, and this antiphase term is refocused at point c. For the magnetization starting from H6, the scalar coupling interaction between C5 and C6 is refocused by adjusting the delay of T to $2/J_{C5\text{-}C6}$. The term $C1'_yN1_z$ (for simplicity, only N1 of pyrimidine is discussed and the chemical shift evolution term is not included) is converted to $C1'_zN1_y$ after the 90° pulse on carbon and nitrogen at point d. From point d to e, continuous decoupling is applied on proton and the chemical shift of N1 is sampled. The I-BURP 180° pulse inverses both C1′ and C6 (also C8 for purine) simultaneously, $C1'_zN1_y$ is evolved into two terms, one giving an out-and-back peak and the other a crossover peak. The out-and-back term is $C1'_zN1_y$ with a factor of $\cos(\pi J_{C1'\text{-}N1}TN)\cos(\pi J_{C6\text{-}N1}TN)$ and the crossover term is $-C6_zN1_y$ with a factor of $\sin(\pi J_{C1'\text{-}N1}TN)\sin(\pi J_{C6-N1}TN)$. From point e to f, the out-and-back and crossover terms are converted to $C1'_yN1_z$ and $-C6_yN1_z$ by the 90° pulse on carbon and nitrogen. Similar to what was described for the coherence transfer from point a to b, the antiphase terms of carbon to nitrogen are refocused from point f to h, the two terms are evolved into $C1'_yH1'_y$ and $-C6_yH6_y$, where the multiple quantum coherence of carbon to the attached proton is generated by the delay of $2\tau_a$ followed by the 90° pulse on the proton at point g. The two terms are further converted to $C1'_zH1'_y$ and $-C6_zH6_y$ after the 90° pulse on carbon at point h. After the last refocusing INEPT step, the chemical shifts of H1′ and H6 are detected during the acquisition. Thus, two peaks starting from H1′ are detected with chemical shifts of, in order of dimension, (C1′, N1 and H1′) and (C1′, N1 and H6). Similarly, two peaks starting from H6 have the chemical shifts of (C6, N1

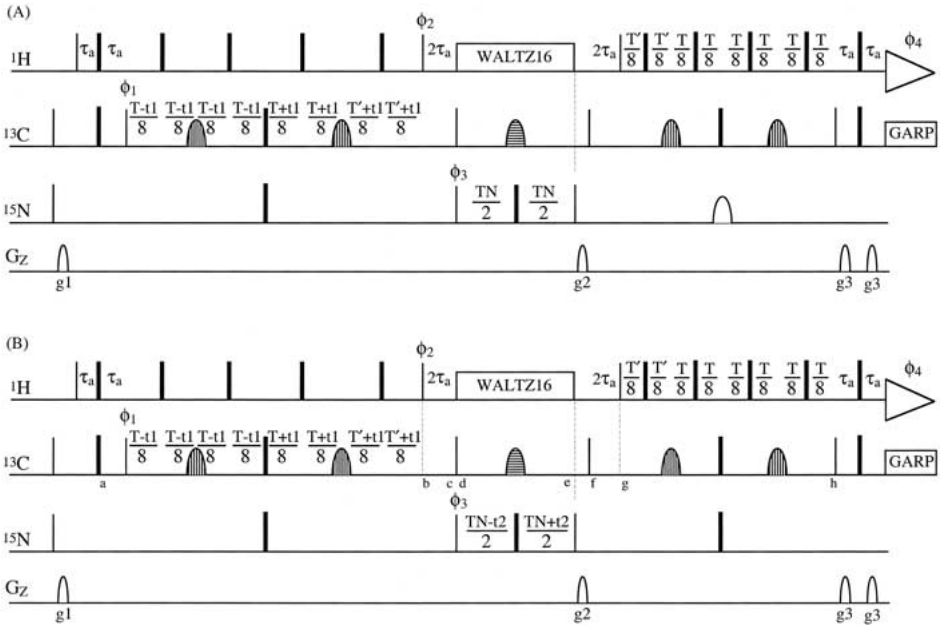

Figure 1. Pulse sequences of the 2D (A) and 3D (B) bi-directional HCNCH experiments for ^{13}C,^{15}N-labeled nucleic acids. Narrow and wide bars represent 90° and 180° pulses, respectively. All pulses are along the x-axis unless otherwise indicated. The shaped pulses filled with vertical bars are off-resonance 180° band-selective I-BURP (Geen and Freeman, 1991) centered at 76 ppm with a duration of 2.3 ms. The shaped pulses filled with horizontal bars are off-resonance 180° band-selective I-BURP centered simultaneously at 91.8 and 140.2 ppm with a duration of 1.9 ms. The blank shaped pulse on nitrogen is 180° on-resonance band-selective I-BURP centered at 148 ppm for the pyrimidine-selected 2D experiment, and at 170 ppm for the purine-selected 2D experiment with the same duration of 4.8 ms. The ^{1}H and ^{13}C carrier frequencies were 4.76, 116 for both 2D and 3D experiments. The ^{15}N carrier frequency was 157.5 ppm for the 3D experiment. Field strengths of the ^{1}H pulse, the ^{13}C high power pulse, the ^{15}N high power pulse and GARP decoupling on ^{13}C (Shaka et al., 1985) were 43.8, 18.5, 6.3, and 4.4 kHz, respectively. Strengths and durations of gradients were g1 = (18 G/cm, 0.2 ms), g2 = (34 G/cm, 0.2 ms), g3 = (18 G/cm, 0.2 ms). $\tau_a = 1.4$ ms, T = 29.8 ms, TN = 25 ms and $T' = T - 8\tau_a$. Phase cycling was ϕ_1 = x, x, −x, −x; ϕ_2 = y, −y; ϕ_3 = 4(x), 4(−x) and Acq. (ϕ_4) = x, −x, −x, x, −x, x, x, −x. Quadrature detection for t_1 was achieved via States-TPPI (Marion et al., 1989) on ϕ_1 for 3A and 3B, and for t_2 on ϕ_3 for 3B.

and H6) and (C6, N1 and H1′). To gain the same information of these correlations, three 3D experiments of those discussed in the introductory part are required. The four peaks of (C1′, H1′), (C6, H1′), (C6, H6) and (C1′, H6) form a rectangular pattern in a carbon-proton plane. The correlation between base and ribose can be realized by any one pair of out-and-back and crossover peaks if no overlaps exist. Under conditions of overlap, the multiple connections among two pairs of out-and-back and crossover peaks make the base-ribose correlation a much less ambiguous process. It is worth noting that the cross and diagonal peaks have opposite signs, and the 1D experiment yields a very weak signal.

The 2D bid-HCNCH experiment (Figure 1A) is very similar to the 3D experiment except that the nitrogen chemical shift is not labeled, and a selective I-BURP 180° pulse on either N1 or N9 is used in the long INEPT step for the refocusing of the carbon antiphase term to the nitrogen. The separation between N1 and N9 is at least more than 10 ppm (Wijmenga and van Buuren, 1998; Hu and Jiang, 1999), and hence a 5 ms I-BURP on a 600 MHz NMR instrument can selectively inverse one group of nitrogens. We have verified the clean selection with 2D N1-H1′ or N9-H1′ correlated spectra on several RNA samples. Selection based on the different chemical shift range of N1 and N9 has been used to simplify the 2D $H_s(C_sN_bC_b)H_b$ spectrum (Gosser et al., 2001). It was noted that if the selective I-BURP 180° on nitrogen was replaced by a hard 180° pulse, strong peaks were observed from the H5-C5-N3 pathway of uridine. Nevertheless, these peaks do not interfere with the data analysis since the N3 of uridine has a different chemical shift range from those of N1/9 (Wijmenga and van Buuren, 1998). The advantages of the N1/9-selected 2D bid-HCNCH are that sub-spectra are much less crowded, high resolution data can be acquired along the carbon dimension, more signal averaging is feasible and data analysis is much simpler.

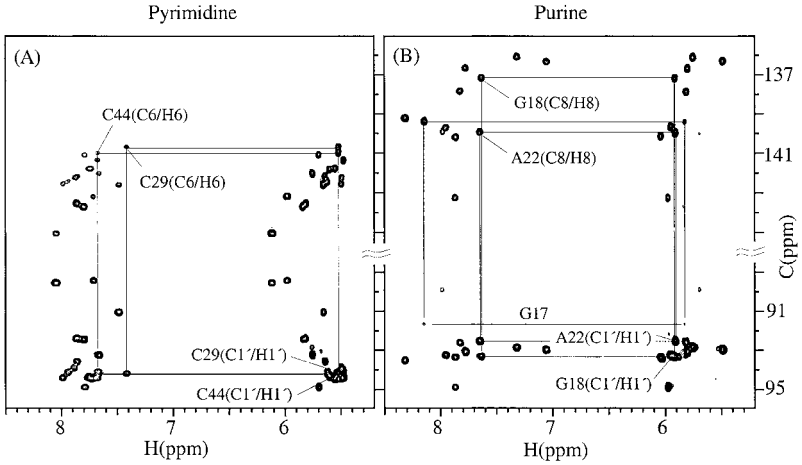

Figure 2. Carbon-proton correlated spectra for pyrimidine (2A) and purine (2B) acquired using the 2D bid-HCNCH sequence (1A) on uniformly $^{13}C/^{15}N$ labeled 27-mer HIV-1 TAR RNA containing a UUCG hairpin loop. The spectral widths (Hz)/no. of complex points for the carbon and proton dimensions were 4375/108 and 8000/544 with 96 transients for (A) and 144 for (B). The total experimental times were 9 and 13.5 h for (A) and (B), respectively. All other related parameters are the same as in the legend to Figure 1. Since chemical shifts of both C1′ and C6/8 are folded, the C1′ regions are located below the C6/8 regions in both spectra. The correlation of base-ribose positions can be found through tracing the individual rectangular pattern outlined by the thin lines.

The pulse sequences of 2D and 3D bid-HCNCH shown in Figure 1 were tested on a 1.6 mM uniformly $^{13}C,^{15}N$-labeled 27-mer TAR RNA fragment, in which the loop CUGGGA was replaced by a stable tetraloop sequence UUCG. This substitution reduces the Tat binding affinity to a small extent (Aboul-ela et al., 1996). The sequence is $G_{17}GCAGAUCUGAGC_{29}U_{31}UCG_{34}G_{36}CUCUCUG CC_{45}$. Two residues (30 and 35) in the sequence were omitted in order to keep the numbers of nucleotides consistent with the wild-type TAR RNA. The sample was dissolved in D_2O at pH 6.1. All the NMR experiments were carried out on a Varian Inova 600 MHz spectrometer equipped with actively shielded performa II Z-gradients at 25 °C. The data was processed and analyzed using NMRPipe (Delaglio et al., 1995) and NMRView (Johnson and Blevins, 1994) software on an SGI O2 workstation.

Shown in Figure 2 are the spectra acquired from the 2D bid-HCNCH sequence with an I-BURP 180° pulse acting on either N1 of pyrimidine (Figure 2A) or N9 of purine (Figure 2B). Clearly, the simplified spectra (Figures 2A and 2B) are much easier to analyze, especially for the regions corresponding to the C1′ positions. To demonstrate the usage of the experiment, C29 and C44 were taken as an example in Figure 2A. Although the chemical shifts of C1′ and H1′ of C29 and C44 are indistinguishable, the base-ribose correlation of these two nucleotides is unequivocal through tracing the two different rectangular connections due to the different chemical shifts of C6 and H6. This is because the chemical shifts of C6 and H6 of these two cytosines are different. Shown in Figure 2B is an example where A22 and G18 share almost identical H1′ and H8 chemical shifts. Since the chemical shifts of C1′ and C8 for these two nucleotides are different, the individual rectangular arrangement is recognizable through the pattern similar to the E. COSY experiment (Griesinger et al., 1985; Eggenberger et al., 1992). In essence, the small difference in chemical shifts of H1′ and H8 becomes distinguishable through the much larger different chemical shifts in the carbon dimension. Actually, the base-ribose correlation of these two nucleotides was not available from the 2D $H_s(C_sN_bC_b)H_b$. Even in the 3D $H_s(C_s)N_b(C_b)H_b$, the necessary resolution for base-ribose correlation of these two nucleotides was not available without the aid of a 3D HCN experiment to sample both H1′-C1′-N1/9 and H6/8-C6/8-N1/9 moieties. By using the 2D bid-HCNCH experiment, all the base-ribose correlations have been assigned for the 27-mer TAR RNA. The crossover peak (H1′, C8) and the out-and-back peak (H1′, C1′) of G36 do not appear in Figure 2B because the chemical shift of H1′ is at 4.44 ppm. There are also some weak peaks in both Figures 2A and 2B due to the presence of minor conformations.

The application of 3D bid-HCNCH is demonstrated in Figures 3A and 3B for the G18 and A22 nucleotides, respectively. The base-ribose correlation of these two nucleotides has been established in the

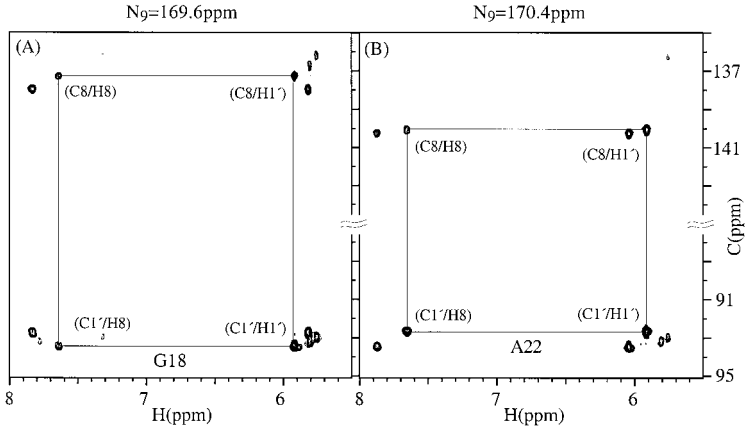

Figure 3. 2D planes of carbon-proton correlation at 169.6 (A) and 170.4 ppm (B) along the nitrogen dimension from the 3D data acquired using 3D bid-HCNCH on uniformly $^{13}C/^{15}N$ labeled 27-mer HIV-1 TAR RNA containing a UUCG hairpin loop. The spectral widths (Hz)/no. of complex points along ^{1}H, ^{13}C and ^{15}N were 8000/544, 4375/44 and 2006/30, respectively, with 32 transients per FID. The total experimental time was 71 h. The resolution of both the ^{13}C and ^{15}N dimensions was enhanced through linear prediction (Delaglio et al., 1995), resulting in a final matrix size of 512×128×128. The correlation of base-ribose of G18 and A22 can be easily obtained through the thin line connections in (A) and (B).

2D bid-HCNCH experiment as discussed above. Nevertheless, their correlation can be further verified from the well-separated individual rectangular patterns in the 3D bid-HCNCH experiment due to their resolved N9 chemical shifts along the nitrogen dimension. The proton-carbon crossover and out-and-back peaks of these two nucleotides are labeled along the rectangular trace in Figures 3A and 3B for G18 and A22, respectively. The 2D planes were taken at 169.6 and 170.4 ppm along the nitrogen dimension.

The sensitivity of heteronuclear correlation experiments correlating base and ribose positions is confined by the small scalar couplings of C1′-N1/9 and C6/8-N1/9. The application of slow relaxation associated with multiple quantum coherence and TROSY techniques improves the sensitivity of HCN and HCNCH significantly and makes this kind of experiment applicable to medium and large-sized nucleic acids. While TROSY can significantly enhance the sensitivity for the carbon-proton pair in aromatic rings, it does not work as well for the C1′/ H1′ pair due to the small CSA of carbons in the ribose ring (Fiala et al., 2000). As a compromise, the multiple quantum coherence of C1′ and C6/8 with respect to the attached proton were adapted during the two long INEPT steps transferring to and back from N1/9. The duration of these two INEPT steps, T, was set to 29.8 ms, which was at the lower end of the values used in the literature (25–42 ms) (Sklenár et al., 1993a; Tate et al., 1994). The reason for the wide range of delay T values is the consideration of carbon-carbon decoupling and transverse relaxation (Wijmenga and van Buuren, 1998). The main purpose for setting T to 29.8 ms in our experiment was to refocus the scalar coupling between C5 and C6 of pyrimidine, which is uniformly ∼67.3 Hz (Wijmenga and van Buuren, 1998). This might not be the optimized value, depending upon the different transverse relaxation rates. The duration of TN was set to 25 ms, and this is a compromise value between the out-and-back and crossover terms associated with factors of $\cos(\pi J_{C1'\text{-}N1/9}TN)\cos(\pi J_{C6/8\text{-}N1/9}TN)$ and $\sin(\pi J_{C1'\text{-}N1/9}TN)\sin(\pi J_{C6/8\text{-}N1/9}TN)$, respectively. The TN value is shorter than the optimized value (32∼40 ms) for one-directional transferred HCNCH-type experiments (Sklenár et al., 1993a; Farmer et al., 1994). Nevertheless, the effect on the sensitivity is not that significant if the T_2 relaxation factor is considered. Quick calculation showed that for a T_2 of 30 ms and 60 ms, when TN changed from 36 ms to 25 ms, the sensitivity was reduced to 96% and 80% , respectively.

The other aspect that should also be considered in evaluating the sensitivity of this experiment compared to other experiments for the base-ribose correlation is the consumption of instrument time. The 3D bid-HCNCH experiment provides five different frequencies (H1′, C1′, N1/9, C6/8 and H6/8), and two ^{13}C-^{1}H crossover peaks for the base-ribose correlation. To gather the same information, usually three different 3D experiments are needed (Sklenár et al., 1993a; Farmer et al., 1993, 1994; Fiala et al., 1998; Riek et al., 2001). This suggests that bid-HCNCH is

a sensitive experiment in the sense of gaining equal information using the same instrument time. Furthermore, the rectangular pattern of the four proton-carbon peaks has more tolerance for the low signal-to-noise in analyzing the data because the peak location is anticipated (Pang et al., 1998). This advantage has been demonstrated on correlating base and ribose of G17 shown in Figure 2B, even though two peaks along the C1′ position are very weak. The weak peaks might be due to the staggered terminus of the RNA.

We applied the 2D bid-HCNCH to a 32-mer RNA oligonucleotide complexed with a 23-residue peptide (Gosser et al., 2001). About 90% of the base-ribose correlations have been assigned with two 2D spectra acquired over a total of 25 h. The complete assignment was curbed by the weak out-and-back peaks of C6/8-H6/8, and less strong crossover peaks of C1′-H6/8. Since the intensity of these peaks is more or less related to the base moiety, the introduction of the TROSY scheme to the sequence should improve the sensitivity of these peaks (Fiala et al., 2000; Riek et al., 2001), and this needs further investigation.

In summary, 2D and 3D bi-directional HCNCH experiments for base-ribose correlation have been presented in this communication. The N1/9 separated 2D bid-HCNCH simplifies the spectrum by a factor of two. It samples four frequencies simultaneously. The use of both proton and carbon dispersions, as well as the rectangular arrangement of the crossover and out-and-back peaks makes the base-ribose correlation less ambiguous and more straightforward. The 3D bid-HCNCH experiment dictates five frequencies with four different types of chemical shift correlation along the H1′-C1′-N1/9-C6/8-H6/8 moiety, which otherwise would require three 3D experiments to achieve. More importantly, it makes data analysis much easier in two aspects: one is the special carbon-proton peak arrangement as discussed above, and the other is that only one 3D matrix needs to be analyzed.

Acknowledgements

This research was funded by NIH grant GM 54777 to D.J.P.

References

Aboul-ela, F., Karn, J. and Varani, G. (1996) *Nucleic Acids Res*., **24,** 3974–3981.

Batey, R.T., Inada, M., Kujawinski, E., Puglisi, J.D. and Williamson, J.R. (1992) *Nucleic Acids Res*., **20**, 4515–4523.

Boelens, R., Burgering, M., Fogh, R.H. and Kaptein, R. (1994) *J. Biomol. NMR*, **4**, 201–213.

Delaglio, F., Grzesiek, S., Vuister, G., Zhu, G., Pfeiffer, J. and Bax, A. (1995) *J. Biomol. NMR*, **6**, 277–293.

Eggenberger, U., Karimi-Nejad, Y., Thuring, H., Rüterjans, H. and Griesinger, C. (1992) *J. Biomol. NMR*, **2**, 583–590.

Farmer II, B.T. and Müller, L. (1991) *J. Magn. Reson.*, **93**, 635–641.

Farmer II, B.T. and Müller, L. (1994) *J. Biomol. NMR*, **4**, 673–687.

Farmer II, B.T., Müller, L., Nikonowicz, E.P. and Pardi, A. (1993) *J. Am. Chem. Soc*., **115**, 11040–11041.

Farmer II, B.T., Müller, L., Nikonowicz, E.P. and Pardi, A. (1994) *J. Biomol. NMR*, **4**, 129–133.

Fiala, R., Czernek, J. and Sklenár, V. (2000) *J. Biomol. NMR*, **16**, 291–302.

Fiala, R., Jiang, F. and Sklenár, V. (1998) *J. Biomol. NMR*, **12**, 373–383.

Geen, H. and Freeman, R. (1991) *J. Magn. Reson*., **93**, 93–141.

Gosser, Y., Hermann, T., Majumdar, A., Hu, W., Frederick, R., Jiang, F., Xu, W. and Patel, D.J. (2001) *Nat. Struct. Biol.*, **8**, 146–150.

Griesinger, C., Sørensen, O.W. and Ernst, R.R. (1985) *J. Am. Chem. Soc*., **107**, 6394–6396.

Grzesiek, S. and Bax, A. (1995) *J. Biomol. NMR*, **6**, 335–339.

Grzesiek, S., Kuboniwa, H., Hinck, A.P. and Bax, A. (1995) *J. Am. Chem. Soc*., **117**, 5312–5315.

Hu, W. and Jiang, L. (1999) *J. Biomol. NMR*, **15**, 289–293.

Johnson, B.A. and Blevins, R.A. (1994) *J. Biomol. NMR*, **4**, 603–614.

Mariani, M., Tessari, M., Boelens, R., Vis, H. and Kaptein, R. (1994) *J. Magn. Reson*., **B104**, 294–297.

Marino, J.P., Diener, J.L., Moore, P.B. and Griesinger, C. (1997) *J. Am. Chem. Soc*., **119**, 7361–7366.

Michnicka, M.J., Harper, J.W. and King, G.C. (1993) *Biochemistry*, **32**, 395–400.

Nikonowicz, E.P., Sirr, A., Legault, P., Jucker, F.M., Baer, L.M. and Pardi, A. (1992) *Nucleic Acids Res*., **20**, 4507–4513.

Pang, Y., Zeng, L., Kurochkin, A.V. and Zuiderweg, E.R.P. (1998) *J. Biomol. NMR*, **11**, 185–190.

Pascal, S.M., Muhandiram, D.R., Yamazaki, T., Forman-Kay, J.D. and Kay, L.E. (1994) *J. Magn. Reson*., **B103**, 197–201.

Riek, R., Pervushin, K., Fernandez, C., Kainosho, M. and Wüthrich, K. (2001) *J. Am. Chem. Soc.*, **123**, 658–664.

Salzmann, M., Ross, A., Czisch, M. and Wider, G. (2000) *J. Magn. Reson.*, **143**, 223–228.

Sattler, M., Maurer, M., Schleucher, J. and Griesinger, C. (1995) *J. Biomol. NMR*, **5**, 97–102.

Shaka, A.J., Barker, P.B. and Freeman, R. (1985) *J. Magn. Reson*., **64**, 547–552.

Sklenár, V., Dieckmann, T., Butcher, S.E. and Feigon, J. (1998) *J. Magn. Reson.*, **130**, 119–124.

Sklenár, V., Peterson, R.D., Rejante, M.R. and Feigon, J. (1993a) *J. Biomol. NMR*, **3**, 721–727.

Sklenár, V., Peterson, R.D., Rejante, M.R., Wang, E. and Feigon, J. (1993b) *J. Am. Chem. Soc.*, **115**, 12181–12182.

Sørensen, O.W. (1990) *J. Magn. Reson*., **89**, 210–216.

Sørensen, O.W., Eich, G.W., Levitt, M.H., Bodenhausen, G. and Ernst, R.R. (1983) *Prog. NMR Spectrosc*., **16**, 163–192.

Tate, S.I., Ono, A. and Kainosho, M. (1994) *J. Am. Chem. Soc*., **116**, 5977–5978.

Wijmenga, S.S. and van Buuren, B.N.M. (1998) *Progr. NMR Spectrosc.*, **32**, 287–387.

Wüthrich, K. (1986) *NMR of Proteins and Nucleic Acids*, Wiley, New York, NY.